Analysis and optimization of gel-cast ceramic foam diesel particulate filter performance

A M Williams[1*], **C P Garner**[1], and **J G P Binner**[2]
[1]Wolfson School of Mechanical and Manufacturing Engineering, Loughborough University, Loughborough, UK
[2]Department of Materials, Loughborough University, Loughborough, UK

The manuscript was received on 22 February 2008 and was accepted after revision for publication on 23 July 2008.

DOI: 10.1243/09544070JAUTO840

Abstract: Gel-cast ceramic foams potentially offer a more robust configurable alternative filtration medium to monolithic wall flow filters (WFFs) for the reduction in particulate matter (PM) emissions from diesel internal combustion engines. The fundamental back pressure and filtration efficiency characteristics of gel-cast ceramic foam diesel particulate filters (DPFs) have been investigated. Methodology is developed for the first time that allows the calculation of the effect of local PM loading on the pressure drop characteristics from experimental data without problems caused by the non-uniform PM loading in the filter that can be applied to all depth bed filtration media. The back pressure and filtration efficiency relationships were used to develop graphical design spaces to aid development of application-specific DPFs. Effects of PM distribution on the pressure drop of the filter are presented. Filters with a non-even distribution of PM were found to have lower pressure drops than filters with an evenly distributed PM for the same average specific PM loadings. The predictions showed that gel-cast ceramic foams can achieve comparable back pressure, filtration volume, and PM holding capacity with WFFs with a lower filtration efficiency of about 80 per cent. The model demonstrated that greater than 90 per cent filtration efficiency can be achieved with filter volumes of about 0.6 times the volume of a WFF with a lower PM holding capacity.

Keywords: diesel particulate filter, gel-cast ceramic foam, back pressure, filtration efficiency, model, depth bed filter, optimization

1 INTRODUCTION

Diesel engine torque characteristics, combustion robustness, thermal efficiency, and large practical bore size range make them widely used for on-highway, off-highway, marine transport, and power generation applications. Combustion in diesel internal combustion (IC) engines generates a number of unwanted by-products including nitrogen oxides (NO_x) and particulate matter (PM). PM emissions from diesel engines have been linked with tumour formation and deoxyribonucleic acid damage following inhalation [**1**, **2**] and are, therefore, a concern in particular within urban areas and industrial environments (e.g. mining industries [**3**]). Increased awareness of the global and local effect of IC engine emissions has led to the restriction of the amount of engine emissions, including diesel PM, by legislative bodies. Significant reductions in PM emissions targets with each legislative cycle are forcing engine manufacturers to consider exhaust gas after-treatment devices [**4**] in addition to in-cylinder techniques such as increased injection pressure [**5**] and exhaust gas recirculation [**6**] to achieve suitable PM and NO_x emissions. This is leading to widespread use of diesel engine exhaust particulate filters.

PM exhaust emissions can be reduced using non-obstructive exhaust systems such as cyclones and electrostatic precipitators. Published literature often demonstrates unfeasibly large systems for mobile applications or, in the case of electrostatic precipitators, requires relatively large amounts of input power to achieve high PM trapping efficiency [**7**].

Corresponding author: Wolfson School of Mechanical and Manufacturing Engineering, Loughborough University, Loughborough, Leicestershire, LE11 3TU, UK. email: a.m.williams@lboro.ac.uk

The interest in these systems is due to their low pressure drop, meaning that the engine pumping losses and negative effects of high exhaust manifold pressures are minimized. To achieve high PM trapping efficiency reliably, obstructive techniques (filtration) are used. Production diesel particulate filters (DPFs) are generally in the form of either a ceramic or metal foam [**8**, **9**] or a monolithic wall flow filter (WFF) [**10**]. WFFs consist of a series of porous walled tubes alternately blocked at the ends which force the gas through the porous wall, filtering the particulates from the gas stream. The average pore diameter of 10–20 μm and porosity of about 50 per cent [**10**, **11**] allow for a period of depth bed filtration before a continuous porous PM layer (the cake layer) is formed on the surface of the filter. This cake layer filters the PM from the exhaust gas with greater than 99 per cent filtration efficiency [**12**]. The structure of the WFF leads to a high surface area, minimizing the back pressure. With a high filtration efficiency and low back pressure these are currently the preferred practical DPF option. Despite these advantages they are readily damaged from uncontrolled thermal regeneration (filter-cleaning) events [**13**] (e.g. because of melting or cracking), and a robust alternative is desirable.

Foam DPFs consist of openly porous structures with typical pore diameters of 100–2000 μm. The pore diameters are larger than WFFs, which causes the PM to be distributed throughout the filter structure (i.e. depth bed filtration). The filtration efficiency is typically about 80 per cent [**8**, **14**, **15**] with back pressures comparable with those of monolithic WFFs [**16**]. The geometry of the filters does not require a large area of thin walls and hence has the potential to be a more robust filtration medium. In addition, the geometry is more flexible, improving the packaging opportunities with a foam DPF in comparison with a WFF.

The development of gel-cast ceramic foams [**17**] and their initial application as a DPF [**18**] demonstrated that they are a promising alternative to both reticulated ceramic foams and monolithic WFFs. Figure 1 shows a typical PM-loaded gel-cast ceramic foam with the characteristic spherical pores. The struts, windows, and pores are highlighted in the image. The manufacturing process of gel-cast ceramic foams results in solid struts that enable the strength of gel-cast ceramic foams to be significantly higher than comparable reticulated ceramic foams (with hollow struts). The solid struts also increase the local thermal conductivity when compared with conventional ceramic foams. It is speculated that the transfer of heat in all directions, rather than along the channel walls (with WFFs) will aid the dissipation of hot spots. The added robustness makes this novel DPF material of value as an alternative to WFFs.

It is well demonstrated in the literature that reducing the pore size increases the filtration efficiency [**8**, **9**, **19**–**24**] since the surface area and sites for PM trapping increase. As the pore size is reduced (and the filtration efficiency increases), the back pressure increases [**20**, **22**, **25**, **26**]. This means that there will be a pore size where the trade-off between the back pressure and filtration efficiency is optimized. This research develops a method that allows evaluation of depth bed particulate filter performance with respect to filtration efficiency and back pressure from a limited amount of filter samples. This requires consideration of the filtration characteristics and back-pressure characteristics as functions of loading.

The demonstrated performance of gel-cast ceramic foams as a promising DPF [**18**] substrate highlighted the need for further research into understanding the filtration properties and optimizing the DPF. The filtration efficiency and back-pressure characteristics of gel-cast ceramic foam DPFs are described, measured, and evaluated in this research. The empirical model used to make projections of the performance of conceptual foam DPFs is valid for all depth bed filtration applications and, therefore, offers a tool that can be used in many filtration material evaluations.

2 EXPERIMENTAL METHOD

A range of pore diameter cylindrical DPF samples in 80 per cent porous cordierite gel-cast ceramic foam

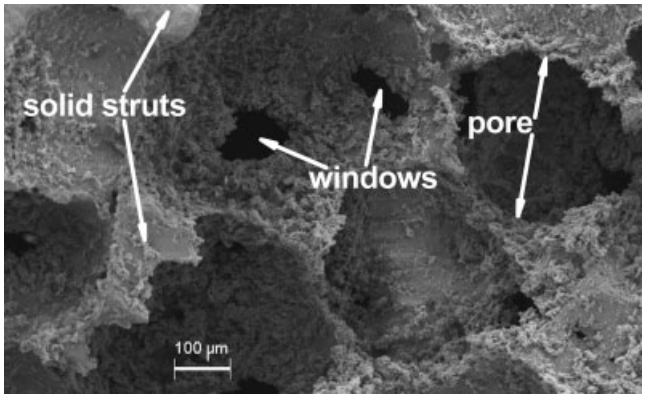

Fig. 1 Scanning electron microscopy image of a PM-loaded gel-cast ceramic foam DPF

Table 1 Test filter specifications

Sample number	Average pore diameter (μm)	DPF diameter (mm)	DPF thickness (mm)
1	290	144	30
2	450	144	30
3	550	144	30
4	680	144	30

Table 2 Test engine specifications [**27**]

Model number	Perkins 1104C-44TA
Peak power (at the engine speed)	92 kW (2200 r/min)
Peak torque (at the engine speed)	475 Nm (1400 r/min)
Number of cylinders	4
Swept volume	4.4 l
Aspiration	Turbocharged
Charge cooling	Simulated air to air
Compression ratio	18.2:1
Bore	105 mm
Stroke	127 mm

were used to generate the data for this study. The details are summarized in Table 1. The methodology developed later in this paper allowed the data from these test samples to be used to make predictions of the performance of conceptual foam geometries and hence evaluate the potential of 80 per cent porous gel-cast ceramic foams.

PM loading is applied to the filters using exhaust flow from a Perkins 4.4 l heavy duty turbocharged charge-cooled diesel engine with specifications listed in Table 2. The purpose-built exhaust canister allowed upstream and downstream measurements of the gas temperature and pressure using K-type thermocouples and calibrated pressure transducers respectively. The location of these measurements is shown schematically in Fig. 2. Gas samples were taken pre- and post-filter to an AVL415 smoke meter to give an estimate of the upstream and downstream PM densities in the exhaust gas using the correlations supplied by the manufacturer.

The filtration efficiency was calculated from the pre- and post-filter AVL smoke meter measurements. The filtration efficiency η was defined as

$$\eta = \left(1 - \frac{\dot{m}_o}{\dot{m}_i}\right) \times 100\% \quad (1)$$

where $\dot{m}_o$ is the downstream mass flowrate of PM and $\dot{m}_i$ is the upstream mass flowrate of PM. With a typical spread of 10 per cent on the smoke meter measurements, uncertainty analysis led to a predicted 95 per cent confidence interval of less than 10 per cent for a filtration efficiency greater than 70 per cent. The confidence interval increased in size for decreasing filtration efficiency.

A controlled hot-gas-flow rig was used to measure the back-pressure characteristics of the gel-cast ceramic foam DPFs. This allowed a wider range of flow conditions to be tested than testing on the engine. A schematic diagram of the hot-flow rig is shown in Fig. 3. A centrifugal blower supplied air flow through a calibrated pitot tube arrangement for measuring the flowrate. This passed through an electrical resistance heater with proportional–integral–derivative control to maintain the test condition gas temperature. This then passed through the filter

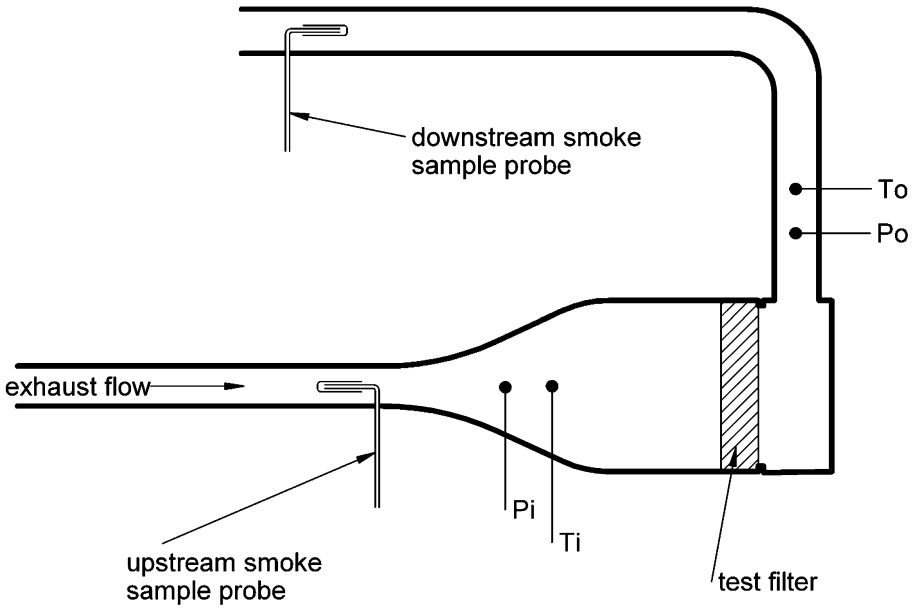

Fig. 2 Schematic diagram of the on-engine filter canister test set-up

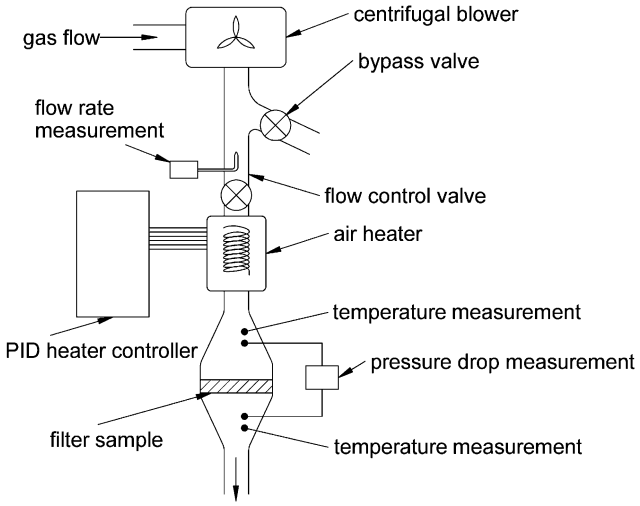

Fig. 3 Schematic diagram showing the key parts of the test rig (PID, proportional–integral–derivative)

sample for which the differential pressure was measured using a digital U-tube manometer to a resolution of 10 Pa and 100 Pa over the ranges 0–10 kPa and 10–20 kPa respectively. The test rig used the same filter mounting procedure and filter sample (with the same PM loading) as the engine test to ensure the results for filtration efficiency and back-pressure characteristics were representative of a single PM loading condition.

3 MODELLING

3.1 Pressure drop

Pressure drop through porous media is known to follow the Forchheimer relationship [**28**] where

$$\frac{\mathrm{d}P}{\mathrm{d}x} = \frac{\mu}{k_1} v + \frac{\rho}{k_2} v^2 \tag{2}$$

where P is the pressure, x is the position through the filter in the direction of the bulk flow, μ is the dynamic viscosity of the gas, v is the gas velocity, ρ is the gas density, and k_1 and k_2 are constants referred to as the viscous coefficient and the kinetic coefficient respectively. The gas is assumed to be compressible (owing to the pressure variation through the filter). Ideal-gas relationships give

$$v = \frac{\dot{V}}{A} = \frac{\dot{m}}{\rho A} = \frac{RT\dot{m}}{PA} \tag{3}$$

where $\dot{V}$ is the volumetric flowrate, A is the frontal surface area of the filter, $\dot{m}$ is the gas mass flowrate, R is the gas constant, and T is the gas temperature. The actual flow distribution across the filter is dependent on the shape of the filter, although for catalytic and filtration applications it will be designed to be as even as possible. To keep the analysis non-prescriptive of filter shape the flow is assumed to be evenly distributed across the filter area. The dynamic viscosity of the gas can be described between 296 K and 1023 K [**29**] as

$$\mu = k_3 T^{0.754} \tag{4}$$

where k_3 is a constant. The Forchheimer relationship can be rewritten in terms of mass flowrate as

$$\frac{\mathrm{d}P}{\mathrm{d}x} = \frac{1}{P}\left(k_4 T^{1.754}\frac{\dot{m}}{A} + k_5 T \frac{\dot{m}^2}{A^2}\right) \tag{5}$$

where k_4 and k_5 are constants. The influence of temperature on the back pressure was checked by evaluating rig data shown in Fig. 4. Quadratic curve fitting and analysis of the fit coefficients allowed calculation of k_4 and k_5 which are shown as functions of temperature in Fig. 5. Within the limits of experimental errors the results can be seen to be almost independent of temperature.

The PM-loaded ceramic foam also follows the Forchheimer relationship, although with different constants k_4 and k_5 (and hence different back pressure). To account for this a polynomial expansion describing the relationship between the coefficients k_4 and k_5 and the local PM loading were used. This means that

$$k_4 = c_{1\mathrm{v}} + c_{2\mathrm{v}}\theta + c_{3\mathrm{v}}\theta^2 + \cdots + c_{m\mathrm{v}}\theta^{m-1} \tag{6}$$

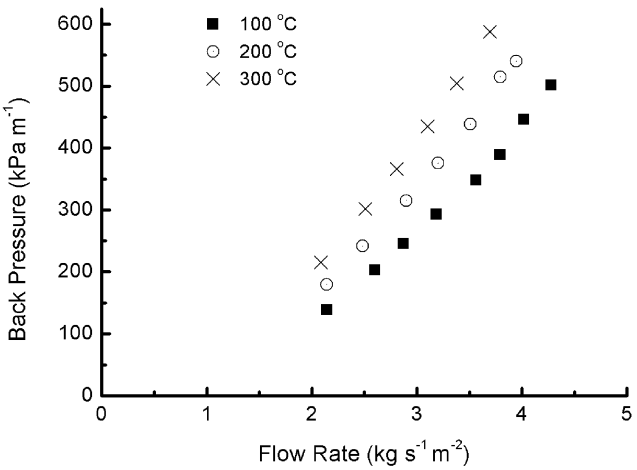

Fig. 4 Effect of the gas temperature on the filter back pressure

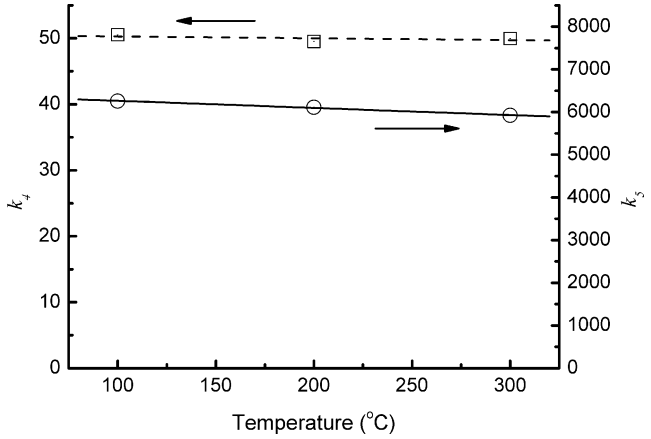

Fig. 5 Plots of the effect of gas temperature on the constants k_4 and k_5

and

$$k_5 = c_{1k} + c_{2k}\theta + c_{3k}\theta^2 + \cdots + c_{mk}\theta^{m-1} \tag{7}$$

where c_{iv} and c_{ik} are constants that are independent of PM loading on the filter and θ is the specific PM loading (g/l). For this study, the relationship between the PM loading and constants k_4 and k_5 was adequately modelled by a quadratic demonstrated later in this paper. The constants are, therefore, defined as

$$k_4 = c_{1v} + c_{2v}\theta + c_{3v}\theta^2 \tag{8}$$

and

$$k_5 = c_{1k} + c_{2k}\theta + c_{3k}\theta^2 \tag{9}$$

The values of c_{iv} and c_{ik} cannot be found directly from experimental data since the gel-cast ceramic foam DPFs cannot be evenly loaded with PM. The exponential loading of the PM through the filter allows average pressure drop measurements across the loaded filter only. Special consideration is therefore required to find the relationship between local PM loading and the filter back-pressure characteristics. To do this, it is necessary to have a relationship describing the distribution of PM along the filtration length.

3.2 PM distribution

The PM distribution is a function of the filtration characteristics of the ceramic foam. It is a complex function of, for example, particle size distribution, flow velocity, and local PM loading. Within this research, a detailed consideration of flow velocity and particle size has not been considered. Test data shown in Fig. 6 imply that the effect of flow velocity in the ranges investigated has a secondary effect when compared with the effect of foam geometry and PM loading. Local PM loading has a large effect and is evident during filter loading tests by the increasing filtration efficiency with time; this must be considered in the analysis. Other effects such as

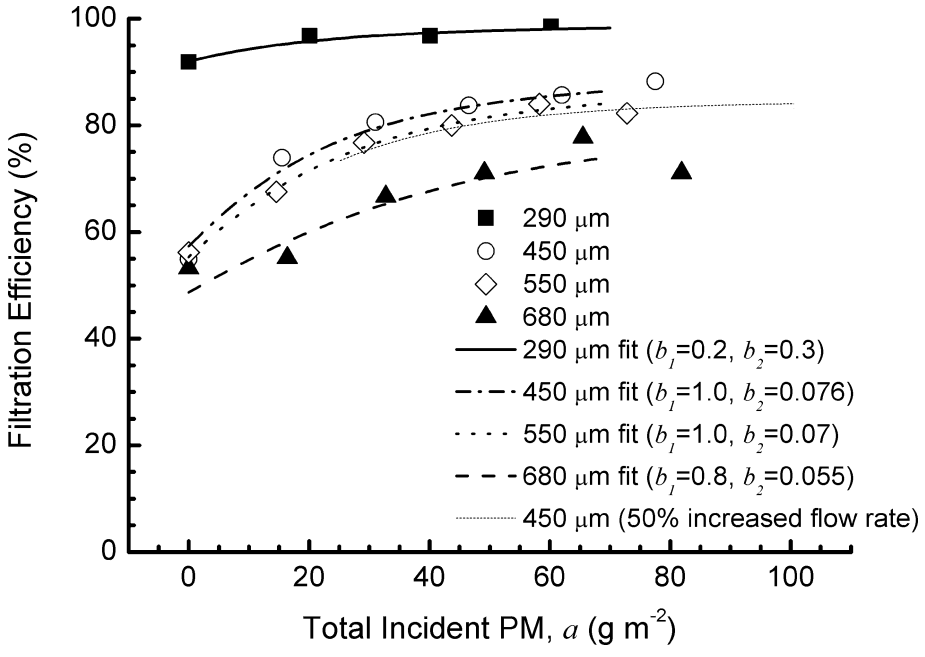

Fig. 6 Temporal filtration efficiency data of gel-cast ceramic foam samples

temperature gradients (thermophoresis) are considered to be negligible in comparison with the previously mentioned factors.

Figure 6 shows typical temporal filtration efficiency characteristics of 80 per cent porous gel-cast ceramic foams of various pore diameters. The filtration efficiency increases with increasing PM loading as the effective pore diameter is reduced and the surface area for trapping increases. Considering the average filtration efficiency trends of the test filters, and understanding that the filtration efficiency will tend towards a maximum at very high loadings, it is reasonable to estimate the effect of PM loading on filtration efficiency to follow the relationship

$$\eta_{\Delta x} = b_1 - (b_1 - \eta_{\Delta x\_c}) \exp(b_2 \theta) \tag{10}$$

where $\eta_{\Delta x}$ is the filtration efficiency of a length Δx of filter with a PM loading of θ, $\eta_{\Delta x\_c}$ is the filtration efficiency of the same length when clean, and b_1 and b_2 are constants. Spatial discretization of a conceptual filter with a given pore structure allows the distribution of PM deposited in the filter from a small amount Δa of incident PM to be predicted. The volume-specific PM deposited in spatial interval n is given by

$$\theta_n = \frac{\Delta a}{t} \eta_{\Delta x,n} \prod_{i=1}^{n-1} (1 - \eta_{\Delta x,i}) \tag{11}$$

Temporal discretization of a loading event (i.e. incrementing the total incident PM a by intervals Δa) allows the prediction of both the distribution of PM through a conceptual filter and the overall filtration efficiency of the filter at a given average loading. After a number m of increments such that the total incident PM is

$$a = m\, \Delta a \tag{12}$$

the local specific loading $\theta_{n,m}$ is

$$\theta_{n,m} = \sum_{j=1}^{m} \theta_{n,j} = \frac{\Delta a}{t} \sum_{j=1}^{m} \left[\eta_{\Delta x,n,j} \prod_{i=1}^{n-1} \left(1 - \eta_{\Delta x,i,j}\right) \right] \tag{13}$$

$\eta_{\Delta x,i,j}$ varies with PM loading and is hence evaluated on the basis of PM loading at the interval $j-1$. It is important to note that the local PM loading is a function of distance from the front face of the filter and the incident PM, and not the overall filter length. The constants b_1 and b_2, therefore, need only be found once for each filter microstructure under investigation.

The constants b_1 and b_2 can found by curve fitting the predicted filtration efficiency using equation (13) to temporal filtration efficiency data from a filter loading on a real engine. An example of these data is shown in Fig. 6, with the curve fits that have been used in the analysis in this research. Constants b_1 and b_2 for each sample are shown in parentheses in Fig. 6.

Equation (13) is used to determine the distribution of PM through a filter of given pore structure and incident PM a. In a more usable continuous form, the PM distribution is approximated as

$$\theta = b_3 \exp\left(-\frac{x}{b_4}\right) + b_5 \tag{14}$$

where b_3, b_4, and b_5 are constants identified from the test data in Fig. 6 to be the values shown in Fig 7.

3.3 Working equations

Combining equations (5), (9), and (14) gives

$$\begin{aligned} P\frac{\mathrm{d}P}{\mathrm{d}x} = {} & \left\{ c_{1\mathrm{v}} + c_{2\mathrm{v}} \left[b_3 \exp\left(-\frac{x}{b_4}\right) + b_5 \right] \right. \\ & \left. + c_{3\mathrm{v}} \left[b_3 \exp\left(-\frac{x}{b_4}\right) + b_5 \right]^2 \right\} T^{1.754} \frac{\dot{m}}{A} \\ & + \left\{ c_{1\mathrm{k}} + c_{2\mathrm{k}} \left[b_3 \exp\left(-\frac{x}{b_4}\right) + b_5 \right] \right. \\ & \left. + c_{3\mathrm{k}} \left[b_3 \exp\left(-\frac{x}{b_4}\right) + b_5 \right] \right\} T \frac{\dot{m}^2}{A^2} \end{aligned} \tag{15}$$

Rearranging gives

$$\begin{aligned} \int P\, \mathrm{d}P = \int \left(\right. & \left\{ c_{1\mathrm{v}} + c_{2\mathrm{v}} \left[b_3 \exp\left(-\frac{x}{b_4}\right) + b_5 \right] \right. \\ & \left. + c_{3\mathrm{v}} \left[b_3 \exp\left(-\frac{x}{b_4}\right) + b_5 \right]^2 \right\} T^{1.754} \frac{\dot{m}}{A} \\ & + \left\{ c_{1\mathrm{k}} + c_{2\mathrm{k}} \left[b_3 \exp\left(-\frac{x}{b_4}\right) + b_5 \right] \right. \\ & \left. \left. + c_{3\mathrm{k}} \left[b_3 \exp\left(-\frac{x}{b_4}\right) + b_5 \right]^2 \right\} T \frac{\dot{m}^2}{A^2} \right) \mathrm{d}x \end{aligned} \tag{16}$$

which, following integration, becomes

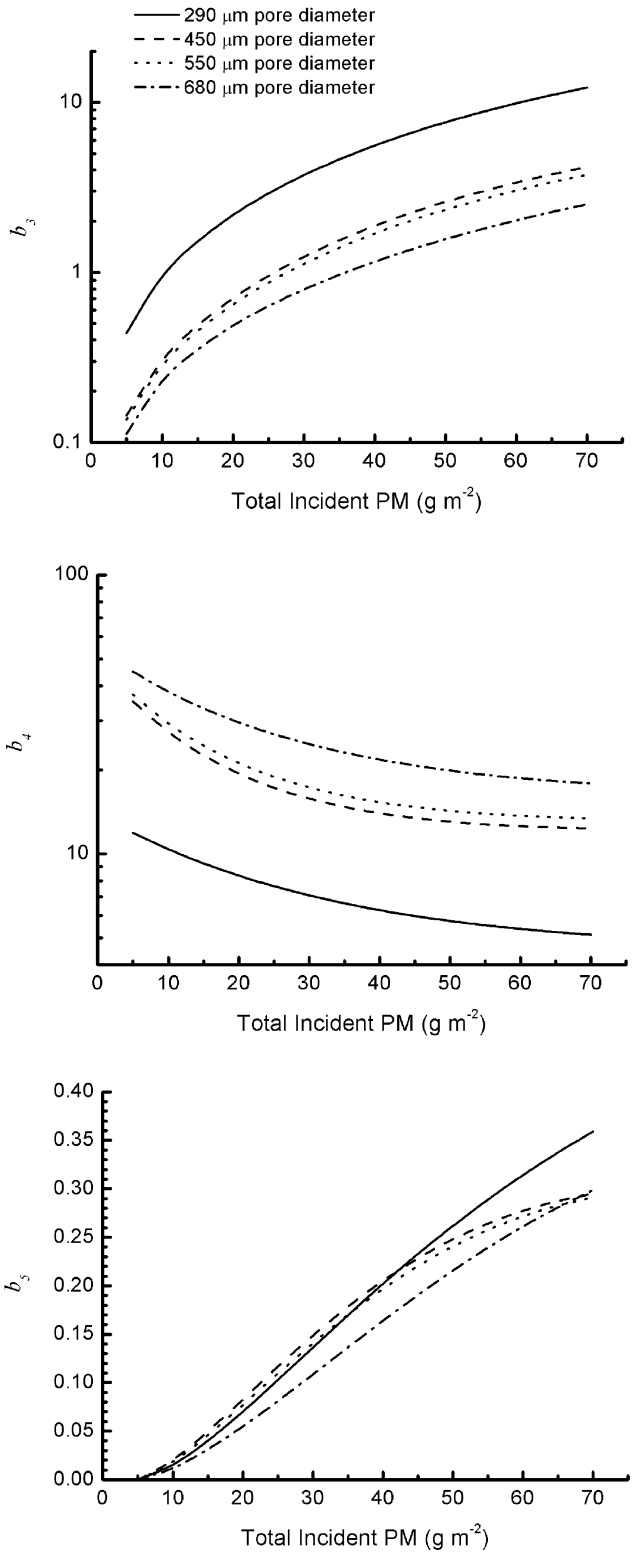

Fig. 7 Constants b_3, b_4, and b_5 as functions of the incident PM

$$\frac{1}{2}P^2 + k_6 = \left\{ c_{1v}x + c_{2v}\left[-b_3b_4 \exp\left(-\frac{x}{b_4}\right) + b_5x \right] + c_{3v}\left[-\frac{{b_3}^2 b_4}{2}\exp\left(-\frac{2x}{b_4}\right) + b_5^2 x - 2b_3b_4b_5 \exp\left(-\frac{x}{b_4}\right) \right] \right\} T^{1.754}\frac{\dot{m}}{A} + \left\{ c_{1k}x + c_{2k}\left[-b_3b_4 \exp\left(-\frac{x}{b_4}\right) + b_5x \right] + c_{3k}\left[-\frac{{b_3}^2 b_4}{2}\exp\left(-\frac{2x}{b_4}\right) + b_5^2 x - 2b_3b_4b_5 \exp\left(-\frac{x}{b_4}\right) \right] \right\} T\frac{\dot{m}^2}{A^2} \quad (17)$$

k_6 can be found by considering the case where $x = 0$, i.e. $P = P_i$, giving

$$k_6 = \left[c_{2v}(-b_3b_4) + c_{3v}\left(-\frac{b_3^2 b_4}{2} - 2b_3b_4b_5 \right) \right] T^{1.754}\frac{\dot{m}}{A} + \left[c_{2k}(-b_3b_4) + c_{3k}\left(-\frac{b_3^2 b_4}{2} - 2b_3b_4b_5 \right) \right] T\frac{\dot{m}^2}{A^2} - \frac{1}{2}P_i^2 \quad (18)$$

where P_i is the upstream gas pressure. Equation (17) becomes

$$\frac{P^2 - P_i^2}{2} = \left(c_{1v}x + c_{2v}\left\{ b_3b_4\left[1 - \exp\left(-\frac{x}{b_4}\right) \right] + b_5x \right\} + c_{3v}\left\{ \frac{b_3^2 b_4}{2}\left[1 - \exp\left(-\frac{2x}{b_4}\right) \right] + b_5^2 x + 2b_3b_4b_5\left[1 - \exp\left(-\frac{x}{b_4}\right) \right] \right\} \right) T^{1.754}\frac{\dot{m}}{A} + \left(c_{1k}x + c_{2k}\left\{ b_3b_4\left[1 - \exp\left(-\frac{x}{b_4}\right) \right] + b_5x \right\} + c_{3k}\left\{ \frac{b_3^2 b_4}{2}\left[1 - \exp\left(-\frac{2x}{b_4}\right) \right] + b_5^2 x + 2b_3b_4b_5\left[1 - \exp\left(-\frac{x}{b_4}\right) \right] \right\} \right) T\frac{\dot{m}^2}{A^2} \quad (19)$$

For a complete filter, where $x = t$, the average PM loading is

$$\begin{aligned}\bar{\theta} &= \frac{1}{t}\int_0^t \theta \, \mathrm{d}x \\ &= \frac{1}{t}\int_0^t \left[b_3 \exp\left(-\frac{x}{b_4}\right) + b_5 \right] \mathrm{d}x \\ &= \frac{1}{t}\left\{ b_3 b_4 \left[1 - \exp\left(-\frac{t}{b_4}\right)\right] + b_5 t \right\} \end{aligned} \tag{20}$$

When squared this gives

$$\begin{aligned}\bar{\theta}^2 = \frac{1}{t^2}\Bigg[& b_3^2 b_4^2 - 2 b_3^2 b_4^2 \exp\left(-\frac{t}{b_4}\right) + 2 b_3 b_4 b_5 t \\ & + b_3^2 b_4^2 \exp\left(-\frac{2t}{b_4}\right) - 2 b_3 b_4 b_5 t \exp\left(-\frac{t}{b_4}\right) \\ & + b_5^2 t^2 \Bigg] \end{aligned} \tag{21}$$

Rearranging gives

$$\begin{aligned}\frac{b_3^2 b_4}{2} \exp\left(-\frac{2x}{b_4}\right) = & \frac{\bar{\theta}^2 x^2}{2b_4} - \frac{b_3^2 b_4}{2} \\ & + \left(b_3^2 b_4 + b_3 b_5 x\right) \exp\left(-\frac{x}{b_4}\right) - b_3 b_5 x - \frac{b_5^2 x^2}{2b_4} \end{aligned} \tag{22}$$

Substituting equations (20) and (22) into equation (19) and simplifying give, for a filter of length t (i.e. $x = t$)

$$\begin{aligned}\frac{P_\mathrm{o}^2 - P_\mathrm{i}^2}{2t} = & \left[c_{1\mathrm{v}} + c_{3\mathrm{v}} B + c_{2\mathrm{v}} \bar{\theta} - \left(\frac{c_{3\mathrm{v}} t}{2b_4}\right)\bar{\theta}^2 \right] T^{1.754} \frac{\dot{m}}{A} \\ & + \left[c_{1\mathrm{k}} + c_{3\mathrm{k}} B + c_{2\mathrm{k}} \bar{\theta} - \left(\frac{c_{3\mathrm{k}} t}{2b_4}\right)\bar{\theta}^2 \right] T \frac{\dot{m}^2}{A^2} \end{aligned} \tag{23a}$$

where

$$\begin{aligned} B = & b_5^2 \left(1 + \frac{1}{2b_4}\right) + \frac{1}{t}\left[1 - \exp\left(-\frac{t}{b_4}\right)\right] \\ & \times \left(b_3^2 b_4 + b_3 b_5 t + 2 b_3 b_4 b_5\right) \end{aligned} \tag{23b}$$

If the quadratic terms in equation (8) and (9) are significant, the pressure drop is not a direct function of the average PM loading but it also depends on the distribution of PM within the filter. The constants c_i were found by analysing data from foam samples at different flowrates and PM mass loadings, without any difficulties posed by the exponential distribution of PM within the test filters.

Assuming that the back pressure is a function of average PM loading only (as is often considered for simplicity), the equivalent equation describing back pressure would be

$$\begin{aligned}\frac{P_\mathrm{o}^2 - P_\mathrm{i}^2}{2t} = & \left(c'_{1\mathrm{v}} + c'_{2\mathrm{v}}\bar{\theta} + c'_{3\mathrm{v}}\bar{\theta}^2\right) T^{1.754} \frac{\dot{m}}{A} \\ & + \left(c'_{1\mathrm{k}} + c'_{2\mathrm{k}}\bar{\theta} + c'_{3\mathrm{k}}\bar{\theta}^2\right) T \frac{\dot{m}^2}{A^2} \end{aligned} \tag{24}$$

4 RESULTS

It was observed that, with the gel-cast ceramic foams with the gas flow velocities tested, the back pressure could be effectively predicted considering only the kinetic term (i.e. proportional to $\dot{m}^2$). A back-pressure indicator and flowrate indicator are defined and were plotted against each other to find the coefficients. The back-pressure indicator is defined as

$$I_\mathrm{BP} = \frac{P_\mathrm{o}^2 - P_\mathrm{i}^2}{2t} \tag{25}$$

and the flowrate indicator is defined as

$$I_\mathrm{flow} = T \frac{\dot{m}^2}{A^2} \tag{26}$$

Equation (23) can now be considered as

$$I_\mathrm{BP} = \left(c_{1\mathrm{k}} + c_{3\mathrm{k}} B + c_{2\mathrm{k}}\bar{\theta} - c_{3\mathrm{k}} \frac{t}{2b_4}\bar{\theta}^2 \right) I_\mathrm{flow} \tag{27}$$

The gradient of the linear fit to a plot of I_BP against I_flow, therefore, yields the term in the parentheses. Figure 8 shows an example plot for three different loadings. A similar analysis was carried out for five different PM loadings on each test sample.

Figure 9 shows how the term in parentheses in equation (27) varies with average specific PM loading. A least-squares fit to the data was used to find the constants c_i. The coefficients from equation (27) are summarized in Fig. 10. These were used to model the performance characteristics of conceptual geometry gel-cast ceramic foam DPFs.

5 MODEL VALIDATION

To validate this method of predicting the back pressure of conceptual gel-cast ceramic foams a sample 144 mm in diameter and 10 mm thick with a 356 μm pore diameter was tested and, using the coefficients from Fig. 10, compared with the predicted back pressure. Figure 11 shows the comparison

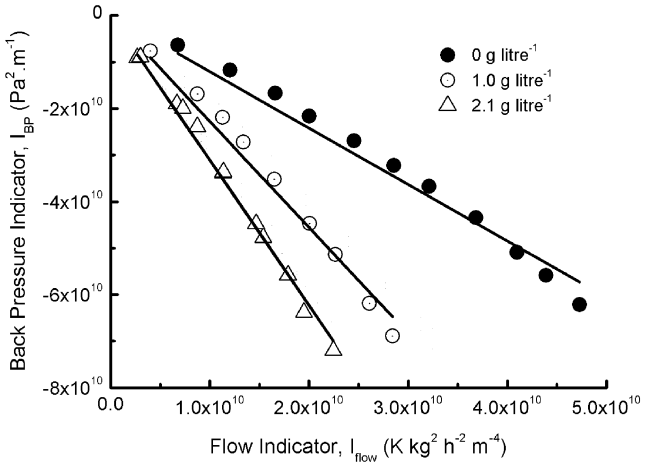

Fig. 8 Back pressure as a function of flowrate and loading for the foam sample of 550 μm pore diameter

of the predicted back pressure from equation (23) with the actual back pressure for the sample.

The sample has a lower surface area than anticipated for application, and the flowrate has been scaled accordingly to give a representative flow velocity. The fit is reasonable, improving with increasing PM loading. The reducing effect of PM loading on the back pressure as PM loading increases is visible in both the experimental data and the predicted data. Equation (23) was, therefore, considered suitable for making predictions of gel-cast ceramic foam DPF performance. The errors in the model are expected to decrease if further samples were used to obtain the characteristics in Fig. 10.

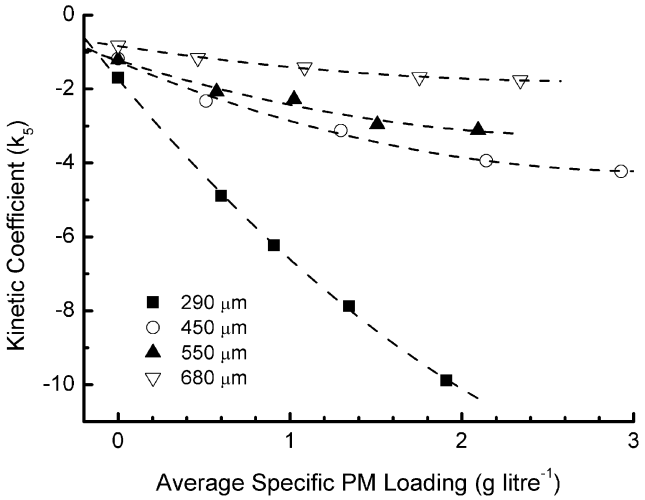

Fig. 9 Plot of the kinetic coefficient as a function of loading

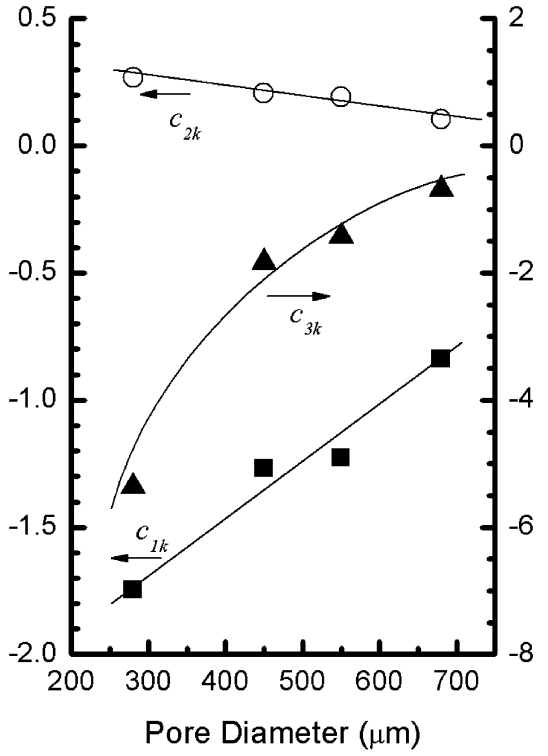

Fig. 10 Plots of the final values of equation constants

Figure 12 compares the experimental data, the prediction from equation (23), and the prediction from equation (24) to demonstrate the effect of considering the PM loading distribution on predictions for a filter sample 20 mm thick. Without consideration of the PM loading distribution the fit can be seen to be an underestimate. This is a function of the difference in filter length when compared with the original test samples in Table 1 and is discussed in more detail later in this paper.

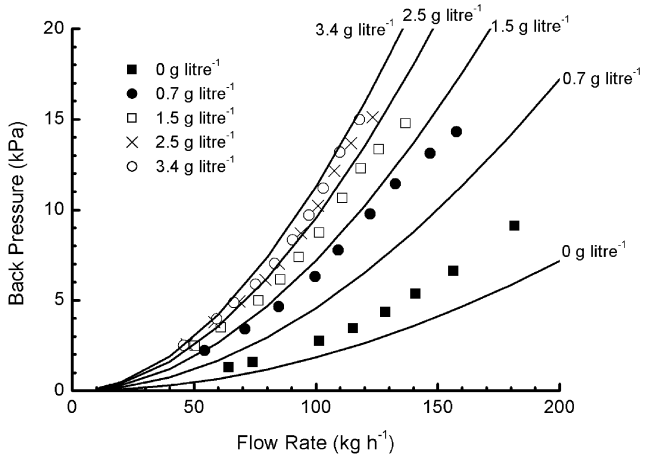

Fig. 11 Comparison of the actual and predicted back pressures of a test foam sample

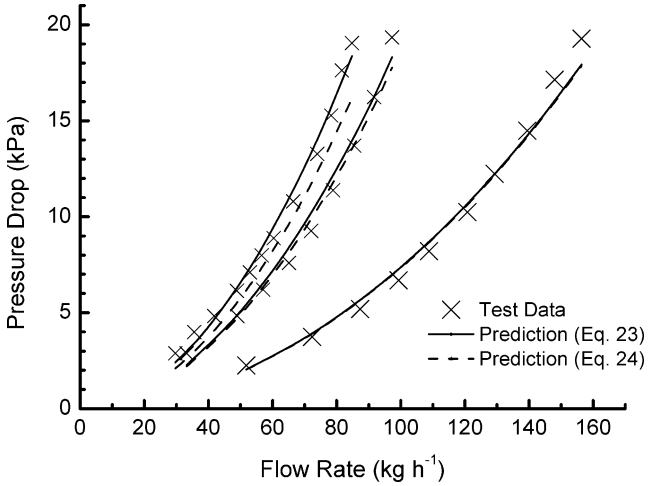

Fig. 12 Comparison of the prediction of equation (23) and equation (24)

6 DISCUSSION

Figure 13 shows the effect of the PM loading distribution when comparing an exponentially loaded foam filter and a (conceptual) evenly loaded foam filter. The deviation represents the difference between the exponentially loaded filter relative to the evenly loaded filter. It shows that, as the average PM loading increases, the non-uniform distribution of PM led to a lower pressure of the DPF. This indicates that the addition of PM to the filter has a larger effect on back pressure with lower PM loadings than with higher PM loadings.

The effects of using equation (23) in comparison with equation (24) was investigated in more detail. Figure 14 shows how the PM loading and filtration thickness of the conceptual foams affected the back-pressure prediction when using equation (23) instead of equation (24). The reference sample had a filtration thickness of 30 mm. This means that, were this based on a real tested sample, that sample would have been 30 mm thick. Figure 14 shows that, with no loading, there is no effect. This was anticipated since the constants c_{lk} are the same in both equations. As the loading increases, the difference between the two equations becomes dependent on the filtration thickness. If the filtration thickness was lower than the reference thickness, equation (23) predicted higher back pressure than using equation (24). For large filtration thicknesses this is reversed and the adequate consideration of PM distribution led to lower predicted back pressure.

To explain this relationship it is necessary to consider Fig. 13 which highlighted that non-uniformity of PM distribution led to lower back pressure. For a filter of a given pore structure the non-uniformity of the PM through the filter is a function of the filtration length. This is demonstrated in Fig. 15 which shows the predicted distribution of PM in the thicker samples to be more non-uniform than with the thinner samples. This directly led to the differences shown in Fig. 14 and demonstrated that, when considering conceptual foam geometries of different filtration thickness than the reference samples, equation (23) should be used to include consideration for the PM distribution within the filter.

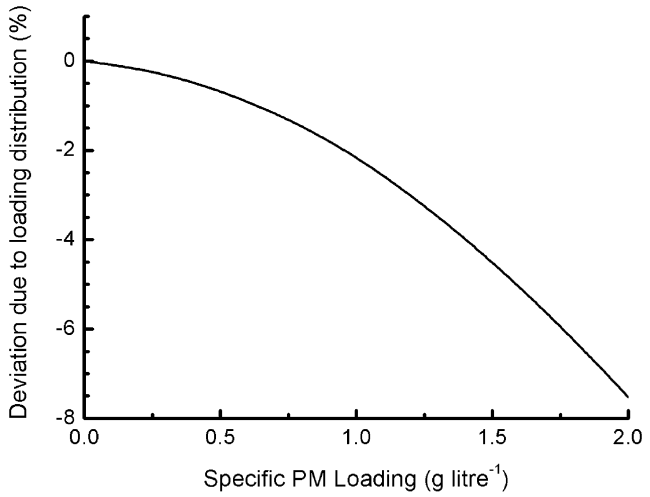

Fig. 13 Comparison of back-pressure prediction of the evenly loaded filter and exponentially loaded filter

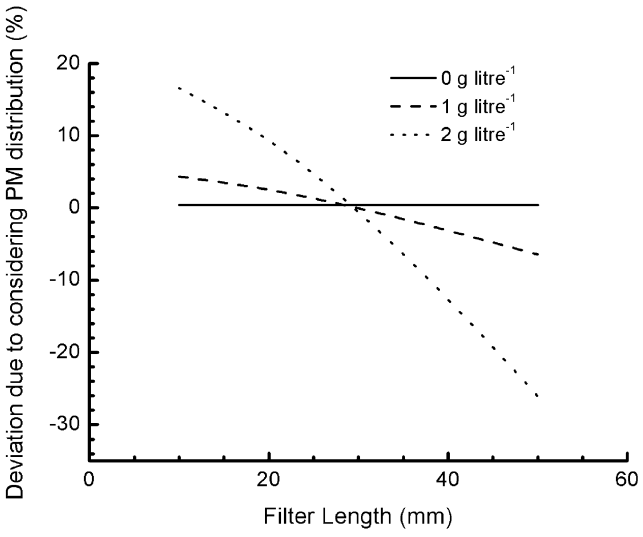

Fig. 14 Effect of considering the PM loading distribution (i.e. equation (23)) on the back-pressure prediction (compared with equation (24))

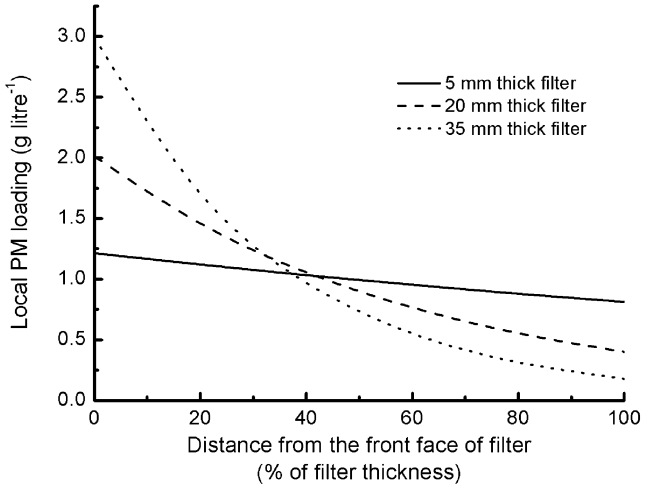

Fig. 15 Effect of filter thickness on the PM distribution

7 DIESEL PARTICULATE FILTER OPTIMIZATION

The back-pressure and filtration efficiency relationships were used to generate design spaces for conceptual foam filter designs. The design space for a 0.06 m^2 frontal area gel-cast ceramic foam DPF is shown in Fig. 16. It shows the following.

1. For a given filtration efficiency, the larger pore size foams require a larger filtration volume (i.e. filtration thickness).
2. For a given filtration efficiency the larger pore size foams offer a higher specific PM holding capacity than smaller pore sizes.
3. For a given pore size foam, reducing the required filtration efficiency reduces the filtration volume and increases the specific PM holding capacity.

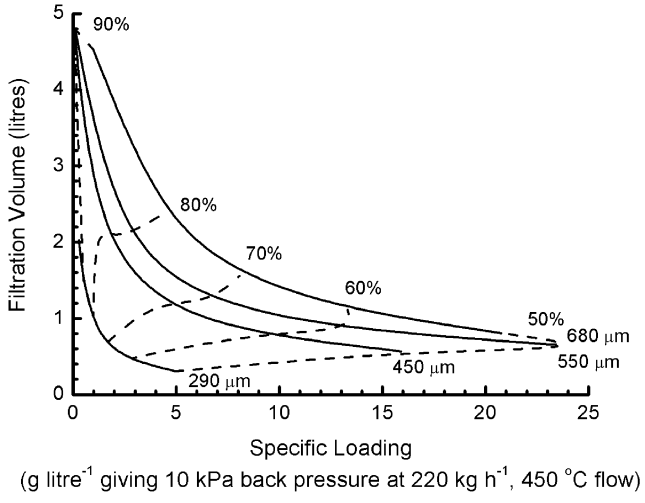

Fig. 16 Design space for a 0.06 m^2 filter

With any two design requirements (out of filtration efficiency, filtration volume, pore size, and specific loading capacity) the design space can be used to determine the other two design parameters. For example, if a filter must have an 80 per cent filtration efficiency and be able to hold up to 3 g/l PM, then the design space can be used to establish that with a 0.06 m^2 filter; the filter would need an average pore diameter of approximately 550 μm, giving a filtration volume of approximately 2.2 l. It is stressed that this analysis does not prescribe a specific filter shape and the 0.06 m^2 filter area is reasonable if packaged as a compact filter shape such as 'top-hat' geometry [**24**].

As with many engineering applications, the optimum design is highly application dependent. It is also noted that the results presented are for 80 per cent porous gel-cast ceramic foams, and further improvements may be achieved by further reducing the foam density. The new design space and methodology presented, however, offer a comprehensive tool to support the design process of gel-cast ceramic foam DPFs. Two examples of gel-cast ceramic foams with different requirements are now presented.

The first example is a filter with a PM holding capacity comparable with that of a WFF with a comparable filtration volume. The design space and equation (23) were used to determine the filtration efficiency and clean filter back pressure of the conceptual foam filter. The data are shown in Table 3. The WFF data were taken from a 100 cpsi 5.66 in diameter filter on the same engine, under the same conditions, with the same test methods. The data are evaluated at mass flow of about 220 kg/h and an exhaust temperature of 450 °C. It can be seen that the clean filter back pressure is acceptable, although higher than that of the WFF, and the filtration efficiency is lower. Despite the lower filtration efficiency it is still high enough to achieve upcoming legislation (based on data for future engine technology NO_x PM trade-off for heavy-duty diesel engines [**4**]). Considering the advantages in filter durability, this shows that gel-cast ceramic foams are a promising option for diesel exhaust particulate filtration.

The performance of a second conceptual filter aiming to achieve 90 per cent filtration efficiency and to minimize packaging volume can also be evaluated from Fig. 16. With a foam of 290 μm pore diameter, a filtration efficiency of 90 per cent can be achieved with a filtration volume of about 1.5 l. This reduction in filtration volume improves packaging,

Table 3 Comparison of an example of gel-cast ceramic foam with monolithic WFF

Parameter (units)	Value for the following	
	Monolithic WFF	Comparable gel-cast foam
Clean filter back pressure (kPa)	≈ 2	≈ 3.5
Loading capacity (g/l)	≈ 6	≈ 6
Filtration size (l)	≈ 2.5	≈ 2.5
Filtration efficiency (%)	> 95	≈ 80

weight, and cost. The disadvantage of such a filter is the low PM holding capacity which would make such a filter more suited to continuously regenerating (filter-cleaning) systems.

8 CONCLUSIONS

In this paper a model has been presented that allows the evaluation of the characteristics of depth bed filters based on experimental data. This has been applied to the case of gel-cast ceramic foam DPFs to understand the filter characteristics in the engine exhaust environment. The investigation of gel-cast ceramic foam DPFs has led to the following important findings.

1. The model and methodology presented in this paper allowed calculation of the effect of local specific PM loading on the pressure drop through the filter.
2. Non-uniform distribution of PM offers lower back pressures than evenly distributed PM of the same average specific PM loading.
3. When evaluating conceptual DPF geometry it is important to consider the distribution of PM.
4. For a given filtration efficiency, the larger pore-size foams require a larger filtration volume (i.e. filtration thickness).
5. For a given filtration efficiency the larger pore-size foams offer a higher specific PM holding capacity than smaller pore sizes do.
6. For a given pore-size foam, reducing the required filtration efficiency reduces the filtration volume and increases the specific PM holding capacity.
7. 80 per cent porous gel-cast ceramic foams can be used as a DPF with a filtration volume and PM holding capacity comparable with those of a WFF with acceptable back-pressure and filtration efficiency.
8. Gel-cast ceramic foam DPFs can be made with smaller filtration volumes than WFFs, although they are limited in the amount of PM that they can hold while maintaining acceptable back pressures.

ACKNOWLEDGEMENTS

The authors gratefully acknowledge the support of Foresight Vehicle, the Department of Trade and Industry, the Department for Transport, Caterpillar (in particular Dave Heaton and Steve Faulkner), Dytech Corporation (in particular Rod Sambrook), and the Engineering and Physical Sciences Research Council during this research.

REFERENCES

1 **Iwai, K., Adachi, S., Takahashi, M., Moller, L., Udagawa, T., Mizuno, S.,** and **Sugawara, I.** Early oxidative DNA damages and late development of lung cancer in diesel exhaust exposed rats. *Environ. Res.*, 2000, **84**, 255–264.

2 **Ma, J. Y. C.** and **Ma, J. K. H.** The dual effect of the particulate and organic components of diesel exhaust particles on the alteration of pulmonary immune/inflammatory responses and metabolic enzymes. *J. Environ. Sci. Health, Part C – Environmental Carcinogenesis Ecotoxic. Rev.*, 2002, **20**, 159–170.

3 **Schnakenberg Jr, G. H.** and **Bugarski, A. D.** Review of technology available to the underground mining industry for control of diesel emissions. DHHS (NIOSH) Publication 2002-154, US Department of Health and Human Services, 2002.

4 **Johnson, T. V.** Diesel emission control in review. SAE technical paper 2008-01-0069, 2008.

5 **Singh, I., Zhong, L., Lai, M.-C.,** and **Henein, N. A.** Effect of nozzle hole geometry on an HSDA diesel engine-out emissions. SAE technical paper 2003-01-0704, 2003.

6 **Kunte, S., Bertola, A., Obrecht, P.,** and **Boulouchos, K.** Temporal soot evolution and diesel engine combustion: influence of fuel composition, injection parameters, and exhaust gas recirculation. *Int. J. Engine Res.*, 2006, **7**, 459–469.

7 **Farzaneh, M., Allaire, M. A., Marceau, K.,** and **Lachance, P.** Electrostatic capture and agglomeration of particles emitted by diesel engines. In the Industry Applications Society Annual Meeting, 1994, Conference Record of the IEEE, 1994, vol. 2, pp. 1534–1537 (IEEE, New York).

8 **Mizrah, T., Maurer, A., Gauckler, L.,** and **Gabathuler, J.-P.** Open-pore ceramic foam as diesel particulate filter. SAE technical paper 890172, 1989.

9 **Barris, M. A., Monson, D. R., Weik, T. M.,** and **Schaefer, J. W.** Material characterisation of diesel particulate trap alternatives. SAE technical paper 872246, 1987.

10 **Miller, P. R., Scholl, J., Bagley, S., Leddy, D.,** and **Johnson, J. H.** The effects of a porous ceramic particulate trap on the physical, chemical and biological character of diesel particulate emissions. SAE technical paper 830457, 1983.

11 **Adler, J.** Ceramic diesel particulate filters. *Int. J. App. Ceram. Technol.*, 2005, **2**(6), 429–439.

12 **Liu, Z. G., Thurow, E. M., Caldow, R.,** and **Johnson, T. R.** Transient performance of diesel particulate filters as measured by an engine exhaust particle size spectrometer. SAE technical paper 2005-01-0185, 2005.

13 **Kitagawa, J., Toshihiko, T.,** and **Makino, M.** Analyses of thermal shock failure on large volume DPF. SAE technical paper 900113, 1990.

14 **Zhi, N., Xinyun, Z.,** and **He, Y.** Development and experimental study of a new diesel exhaust particulate trap system. SAE technical paper 2000-01-2846, 2000.

15 **Boretto, G., Debenedetti, M., Marzorati, D.,** and **Vaglieco, B. M.** Diesel particulate filter based on ceramic foams. SAE technical paper 1999-24-0052, 1999.

16 **Gabathuler, J. P., Mizrah, T., Eckert, L., Fischer, A., Käser, P.,** and **Maurer, A.** New developments of ceramic foam as a diesel particulate filter. SAE technical paper 910325, 1991.

17 **Sepulveda, P.** and **Binner, J. G. P.** Processing of cellular ceramics by foaming and *in-situ* polymerisation of organic monomers. *J. Eur. Ceram. Soc.*, 1999, **19**, 2059–2066.

18 **Hughes, S. W.** *The use of gel cast ceramic foams as diesel particulate filters*. PhD Thesis, Loughborough University, UK, 2003.

19 **Ambrogio, M., Saracco, G.,** and **Specchia, V.** Combining filtration and catalytic combustion in particulate traps for diesel exhaust treatment. *Chem. Engng Sci.*, 2001, **56**, 1613–1621.

20 **Shinozaki, O., Shinoyama, E.,** and **Saito, K.** Trapping performance of diesel particulate filters. SAE technical paper 900107, 1990.

21 **Tutko, J. J., Lestz, S. S., Brockmeyer, J. W.,** and **Dore, J. E.** Feasibility of ceramic foam as a diesel particulate trap. SAE technical paper 840073, 1984.

22 **Watabe, Y., Irako, K., Miyajima, T., Yoshimoto, T.,** and **Murakami, Y.** 'Trapless' trap – a catalytic combustion system of diesel particulates using ceramic foam. SAE technical paper 830082, 1983.

23 **Xu, X., Gao, X., Li, C.,** and **Wang, X.** Aftertreatment for reduction of diesel exhaust particulate. SAE technical paper 2001-01-3204, 2001.

24 **Adigio, E. M.** *Modelling gas flow pressure gradients in gelcast ceramic foam diesel particulate filters*. PhD Thesis, Loughborough University, UK, 2005.

25 **Ciambelli, P., Palma, V., Russo, P.,** and **Vaccaro, S.** Deep filtration and catalytic oxidation: an effective way for soot removal. *Catalysis Today*, 2002, **73**, 363–370.

26 **Helferich, R. L.** and **Schenck, R. C.** Evaluation of a stacked element diesel particulate trap using a newly developed membrane covered ceramic foam filtering media. SAE technical paper 890787, 1989.

27 Perkins 1104C-44TA diesel engine datasheet. Document 1645/02/06, Perkins Engines, Peterborough, UK, 2005.

28 **Innocentini, M. D. M., Salvini, V. R., Macedo, A.,** and **Pandolfelli, V. C.** Prediction of ceramic foams permeability using Ergun's equation. *Mater. Res.*, 1999, **2**(4), 283–289.

29 **Forsythe, W. E.** *Smithsonian physical tables,* 9th revised edition, 2003 (Knovel, Norwich, New York).

APPENDIX

Notation

a	incident particulate matter
A	frontal area of the filter
b	constants
c	constants
I_{BP}	back-pressure indicator
I_{flow}	flowrate indicator
k	constants
$\dot{m}$	mass flowrate of gas
$\dot{m}_i$	upstream particulate matter mass flowrate
$\dot{m}_o$	downstream particulate matter mass flowrate
P	pressure
P_i	upstream pressure
P_o	downstream pressure
R	gas constant
t	thickness of the test filter
T	temperature
v	gas space velocity
$\dot{V}$	volumetric flow rate
x	distance into the filter
η	filtration efficiency
$\eta_{\Delta x}$	filtration efficiency for x mm filtration length
$\eta_{\Delta x\_c}$	filtration efficiency for x mm filtration length when clean
θ	specific loading
μ	dynamic viscosity
ρ	density